CHEMISTRY & SUSTAINABILITY

CHEMSUSCHEM

ENERGY & MATERIALS

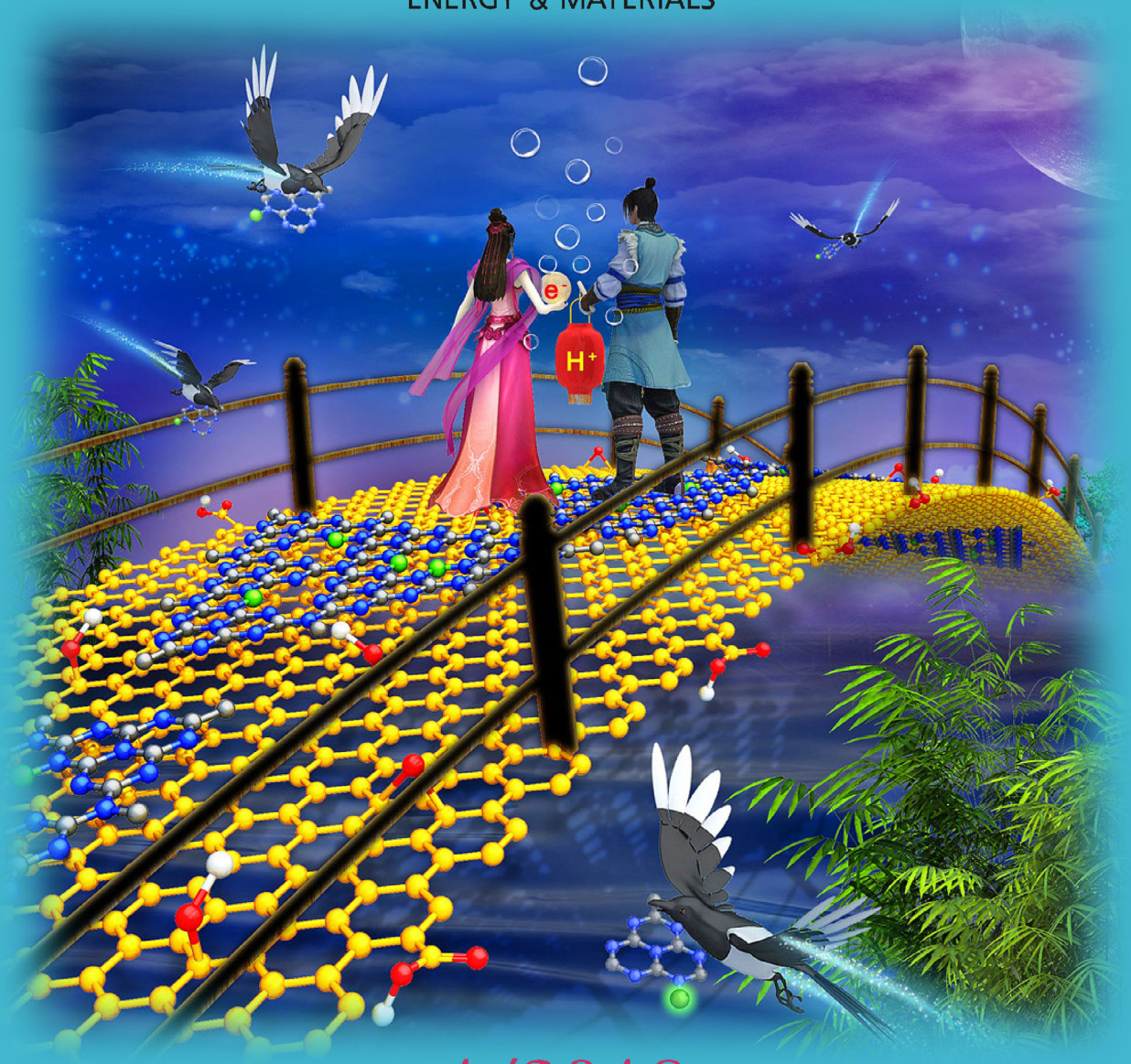

1/2018

Front Cover:

Peng et al.

Ruthenium Ion-Complexed Graphitic Carbon Nitride Nanosheets Supported on Reduced Graphene Oxide as High-Performance Catalysts for Electrochemical Hydrogen Evolution

A Journal of

ChemPubSoc Europe

WILEY-VCH

www.chemsuschem.org

COVER PICTURE

*Y. Peng, W. Pan, N. Wang, J.-E. Lu, S. Chen**

■■ – ■■

Ruthenium Ion-Complexed Graphitic Carbon Nitride Nanosheets Supported on Reduced Graphene Oxide as High-Performance Catalysts for Electrochemical Hydrogen Evolution

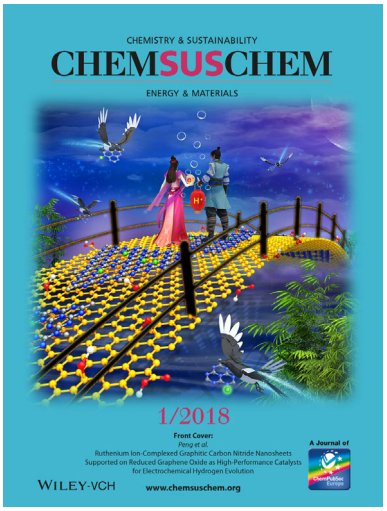

The Front Cover shows the production of hydrogen gas when electrons and protons meet on ruthenium ion-complexed graphitic carbon nitride nanosheets supported on graphene surface. The image is based on an ancient Chinese legend of Niulang (牛郎) and Zhinü (织女). Niulang was a human cowherd and Zhinü was a fairy from heaven. They fell in love with each other. Yet their love was banned by the fairy's queen, who forcefully separated them by the Silver River. The lovers were only able to see each other once a year, on the 7th day of the 7th lunar month, with the help of a flock of magpies that formed a bridge. More information can be found in the Full Paper by Peng et al.

ChemPubSoc Europe

DOI: 10.1002/cssc.201701880

CHEMSUSCHEM Full Papers

Ruthenium Ion-Complexed Graphitic Carbon Nitride Nanosheets Supported on Reduced Graphene Oxide as High-Performance Catalysts for Electrochemical Hydrogen Evolution

Yi Peng,[a] Wanzhang Pan,[a] Nan Wang,[b] Jia-En Lu,[a] and Shaowei Chen*[a]

Carbon-based materials are promising, low-cost electrocatalysts toward hydrogen evolution reaction (HER), although the catalytic performance needs to be further improved before commercialization. In this study, ruthenium ions are incorporated into graphitic carbon nitride/reduced graphene oxide (rGO) hybrids to form Ru–C_3N_4/rGO composites through Ru–N coordination bonds. The incorporation of Ru ions, at a loading of 1.93 at.%, leads to electron redistribution within the materials and dramatically enhances the HER performance over those of C_3N_4, C_3N_4/rGO, and Ru–C_3N_4, with an overpotential of only −80 mV to reach a current density of 10 mA cm^{-2}, a Tafel slope of 55 mV dec^{-1}, and an exchange current density of 0.462 mA cm^{-2}. This performance is comparable to that of Pt/C, and ascribed to the positive shift of the conduction band of the composite, where the charge carrier density increases by a factor of about 250 over that of C_3N_4, leading to a lower energy barrier for hydrogen evolution. The results suggest a new strategy in the design and engineering of functional nanocomposites for effective HER electrocatalysis by embedding select metal ions into carbon-based molecular skeletons.

Introduction

As a clean and environmentally friendly fuel, hydrogen has been hailed as one of the most promising energy sources of the future. Towards this end, it is imperative to develop efficient technologies for hydrogen storage and conversion.[1,2] Mechanistically, effective electrocatalysts are required to achieve a high hydrogen generation rate as the hydrogen evolution reaction (HER) involves multiple electron-transfer steps.[3,4] To date, platinum-based materials supported on carbon have exhibited the best electrocatalytic performance for HER. However, widespread commercial applications are hindered by the low natural abundance and high costs of platinum.[5] In recent years, a variety of transition metal-based materials have been found to show apparent electrocatalytic activities towards HER. However, durability remains an issue because of corrosion of the catalysts in acidic electrolytes, a common medium for HER.[6–9] Carbon-based materials, such as graphene, carbon nanotubes, and amorphous carbon, have also been explored as viable catalysts for HER.[10–18] However, their activities have remained markedly lower than that of state-of-the art Pt/C.

More recently, Chhetri et al. found that carbon-rich borocarbonitrides (BC_7N_2) had an apparent activity with an overpotential (η_{10}) of only −70 mV to reach a current density of 10 mA cm^{-2}, which was comparable to that of Pt/C. However, the Tafel slope was relatively high (100 mV dec^{-1}), indicative of increasing deviation from Pt/C at high overpotentials.[19] In another study,[20] carbon nitride (C_3N_4) and N-doped graphene (NG) were combined to form a hybrid structure that exhibited apparent HER activity arising from electronic coupling between C_3N_4 and NG. However, the η_{10} value remained quite high at −240 mV. The HER performance may be enhanced by morphological engineering of C_3N_4 and graphene, but it is difficult to reduce η_{10} to below −200 mV.[21–23] In a more recent study,[24] we showed that when ruthenium metal ions were embedded into C_3N_4 nanosheets, the resulting Ru–C_3N_4 complex exhibited much-enhanced HER activity. This was accounted for by the formation of Ru–N coordination bonds, owing to the strong affinity of ruthenium(II) ions to pyridinic nitrogen of the tri-*s*-triazine units of C_3N_4 that facilitated the adsorption and reduction of hydrogen with an η_{10} of −140 mV and Tafel slope of 57 mV dec^{-1}, whereas only minimal activity was observed with other metal ions, such as Fe^{3+}, Co^{3+}, Ni^{3+}, and Cu^{2+}.[24]

In the present study, the HER performance was further improved by incorporating graphene into the Ru–C_3N_4 complex. Experimentally, C_3N_4 nanosheets were mixed with reduced graphene oxide (rGO) and then embedded with ruthenium metal ions by thermal refluxing of $RuCl_3$ in water (Scheme 1). Despite a low Ru loading of only 1.93 at.%, the resulting Ru–C_3N_4/rGO nanocomposite exhibited markedly enhanced electrocatalytic activity towards HER over those of the individual components

[a] Y. Peng, W. Pan, J.-E. Lu, Prof. Dr. S. Chen
Department of Chemistry and Biochemistry, University of California
156 High Street, Santa Cruz, CA 95064 (USA)
E-mail: shaowei@ucsc.edu

[b] N. Wang
New Energy Research Institute, School of Environment and Energy
South China University of Technology
Guangzhou Higher Education Mega Centre, Guangzhou 510006 (China)

Supporting information and the ORCID identification number(s) for the author(s) of this article can be found under https://doi.org/10.1002/cssc.201701880.

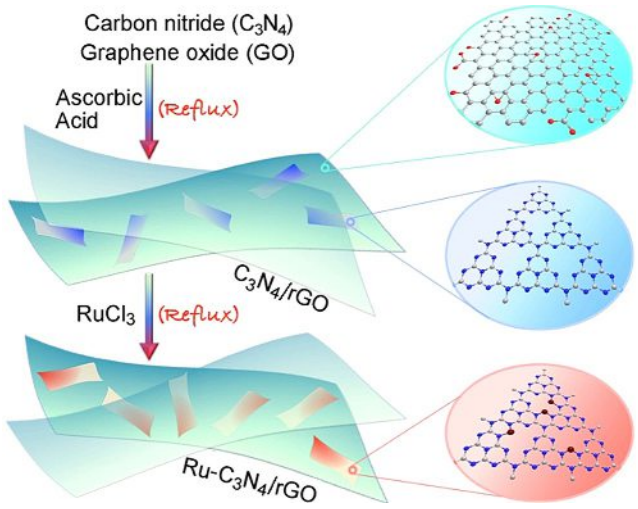

Scheme 1. Schematic illustration of the preparation of Ru–C_3N_4/rGO nanocomposites.

and their binary composites, with a low η_{10} of only −80 mV, a Tafel slope of 55 mV dec^{-1}, and an exchange current density of 0.462 mA cm^{-2}. Notably, this performance is comparable to that of Pt/C.

Results and Discussion

The synthesis of the Ru–C_3N_4/rGO hybrid is shown in Scheme 1. Briefly, GO was prepared by a modified Hummers method by using graphite flakes as precursors,[25,26] and C_3N_4 nanosheets were synthesized by sonication of graphitic C_3N_4 obtained by thermal treatment of melamine in air.[27,28] Refluxing of the mixture of C_3N_4 and GO in water with the addition of ascorbic acid led to the production of C_3N_4/rGO composites, likely in the form of a sandwich structure.[20,21,29] With the addition of a calculated amount of $RuCl_3$ into the solution, ruthenium metal ions were incorporated into the nanocomposites by complexation with the pyridinic nitrogen of the tri-*s*-triazine units of the C_3N_4 scaffolds, forming Ru–C_3N_4/rGO hybrid materials.

The formation of the composites was first confirmed by atomic force microscopy (AFM) topographic measurements, from which one can see that C_3N_4 nanosheets are well-dispersed without apparent aggregation (Figure 1 a_1). Line scans show that the nanosheets are about 2 nm in thickness (Figure 1 a_2). Statistical analysis based on more than 100 nanosheets shows that the average thickness is 2.0 ± 0.4 nm (see the histogram in Figure 1 a_3), corresponding to roughly 6 layers in C_3N_4 (interlayer spacing of C_3N_4 is about 0.33 nm).[24] With

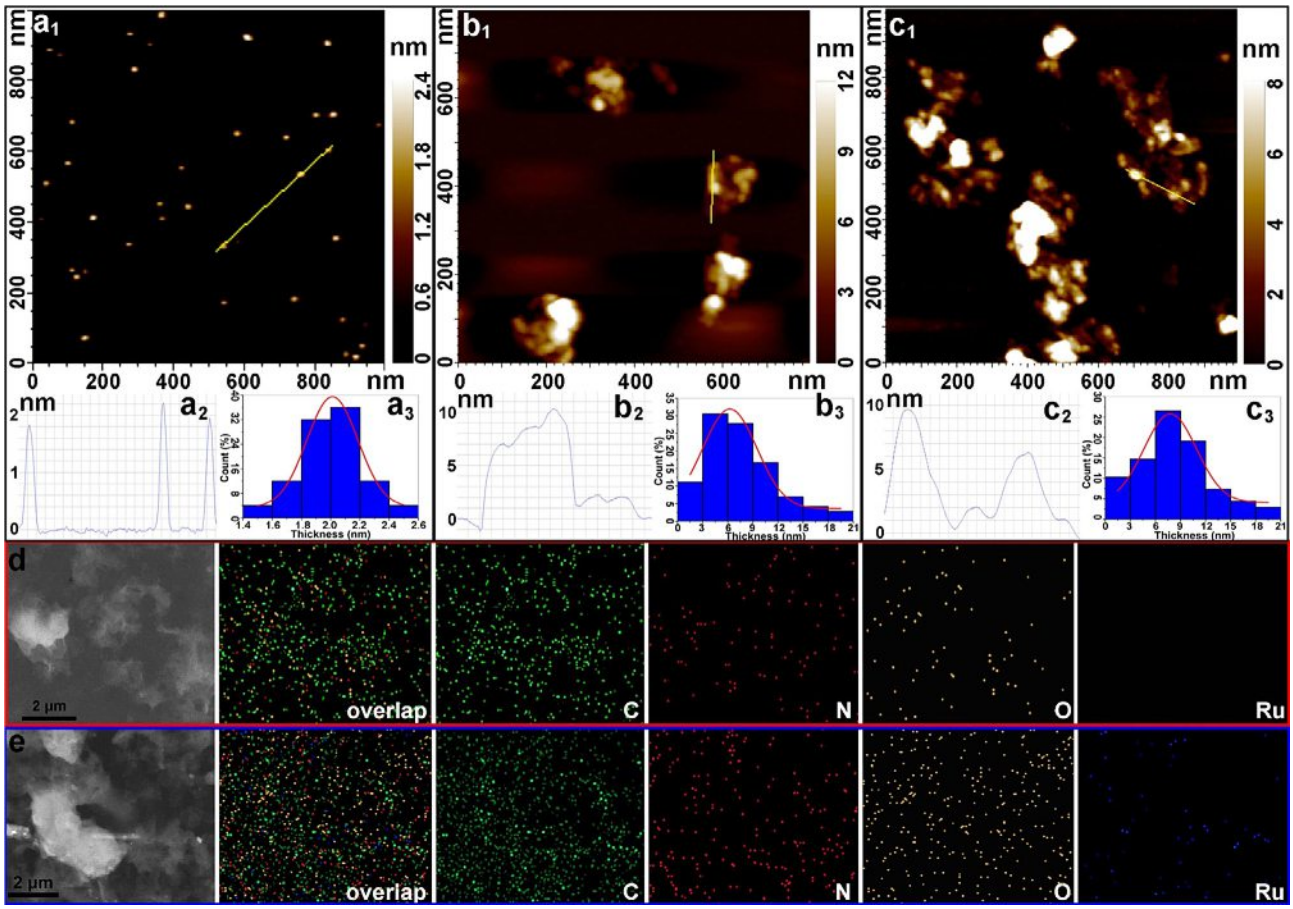

Figure 1. a–c) Representative AFM topographes of (a_1) C_3N_4, (b_1) C_3N_4/rGO composites, and (c_1) Ru–C_3N_4/rGO complex, the corresponding height profiles of the lines scans (a_2, b_2, and c_2), and thickness histograms of the samples (a_3, b_3, and c_3). d, e) Representative TEM images and the corresponding elemental maps of carbon, nitrogen, oxygen and ruthenium of (d) C_3N_4/rGO and (e) Ru–C_3N_4/rGO nanocomposites.

the addition of rGO, substantial aggregation occurred with the resulting C_3N_4/rGO composites (Figure 1 b_1), and the thickness increased markedly up to 10 nm (Figure 1 b_2), with an average of 6.3 ± 3.7 nm (Figure 1 b_3). This is likely due to the formation of C_3N_4/rGO sandwich-like ensembles as a result of strong π–π interactions between the C_3N_4 and rGO nanosheets (Figure S1 in the Supporting Information).[29–32] Notably, no apparent variation was observed with the morphology or thickness of the nanocomposites after the embedment of ruthenium ions into the C_3N_4 scaffold (Figure 1 c). From the TEM images of the C_3N_4/rGO and Ru–C_3N_4/rGO nanocomposites and the corresponding elemental maps (Figure 1 d, e), one can see that no particulate materials were produced, that both C_3N_4/rGO and Ru–C_3N_4/rGO exhibited similar agglomeration, and that all elements were distributed evenly across the respective samples. Note that although Ru was not detected in C_3N_4/rGO, the signals were quite visible for Ru–C_3N_4/rGO.

Further structural insights were obtained by X-ray photoelectron spectroscopy (XPS). Figure 2 a depicts the survey spectra of (i) C_3N_4, (ii) C_3N_4/rGO, and (iii) Ru–C_3N_4/rGO, where the peaks at 284, 399, and 531 eV may be assigned to the C 1s, N 1s, and O 1s electrons, respectively. In addition, the peak at 464 eV in curve (iii) for Ru–C_3N_4/rGO, which is absent in those for the other two samples, can be ascribed to Ru 3p electrons (Ru 3d overlaps with C 1s),[33] suggesting that indeed ruthenium metal ions were successfully incorporated into the nanocomposites. Furthermore, based on the integrated peak areas, the elemental composition in Ru–C_3N_4/rGO can be estimated to be 67.88 at.% for C, 7.48 at.% for N, 22.75 at.% for O and 1.93 at.% for Ru (see the Supporting Information, Table S1). From the high-resolution spectra (Figure 2 b), deconvolution yields a major peak at 287.40 eV for C_3N_4 (curve i) that may be assigned to the sp^2-hybridized carbon in N–C=N and a minor one at 284.20 eV from defective carbon.[34] For C_3N_4/rGO (curve ii) and Ru–C_3N_4/rGO (curve iii), the N–C=N peak shifted positively to 287.85 and 288.02 eV, respectively, indicating reduced electron density of the sp^2 C in C_3N_4, likely due to charge transfer from C_3N_4 to rGO and/or Ru centers.[35] Two additional peaks can be identified at 284.31 and 286.16 eV, which may be ascribed to carbon in C=C and C–O of rGO, respectively. The peaks are somewhat lower than those observed with rGO alone (C=C at 284.60 eV and C–O at 286.50 eV), suggesting enhanced electron density of these carbon moieties.[36] For the Ru–C_3N_4/rGO sample (Figure 2 b, curve iii), deconvolution also yields a doublet at 281.96 and 286.16 eV that is very consistent with the $3d_{5/2}$ and $3d_{3/2}$ electrons of Ru^{II} ions in Ru–N moieties, indicating that Ru^{III} was reduced to Ru^{II} during the refluxing process, most probably by hydroxy species,[37] and incorporated into the C_3N_4 matrix by Ru–N coordination bonds.[24,38] Figure 2 c shows the N 1s spectra, where two subpeaks can be resolved in all three samples. For C_3N_4 (curve i), the peak at 397.86 eV may be assigned to sp^2-hybridized pyridinic nitrogen (C–N=C) and that at 399.62 eV to sp^3-hybridized tertiary nitrogen (NC_3).[39] For C_3N_4/rGO (curve ii) and Ru–C_3N_4/rGO (curve iii), the C–N=C peak had undergone an apparent blueshift to 398.47 eV and 398.65 eV, respectively. Taken together, these results suggest efficient charge transfer from C_3N_4 to rGO and Ru centers.[24,29,40,41] Furthermore, based on the integrated peak areas, the atomic ratio of N (C–N=C) to Ru was estimated to be approximately 2.3 for the Ru–C_3N_4/rGO sample, similar to that observed previously with Ru–C_3N_4 where the ruthenium ions were coordinated to two N sites in C–N=C.[24] Overall, results from the XPS measurements suggested strong electronic interactions among the three structural components of Ru–C_3N_4/rGO, which may have significant impacts on the electrocatalytic activity towards HER (see below).

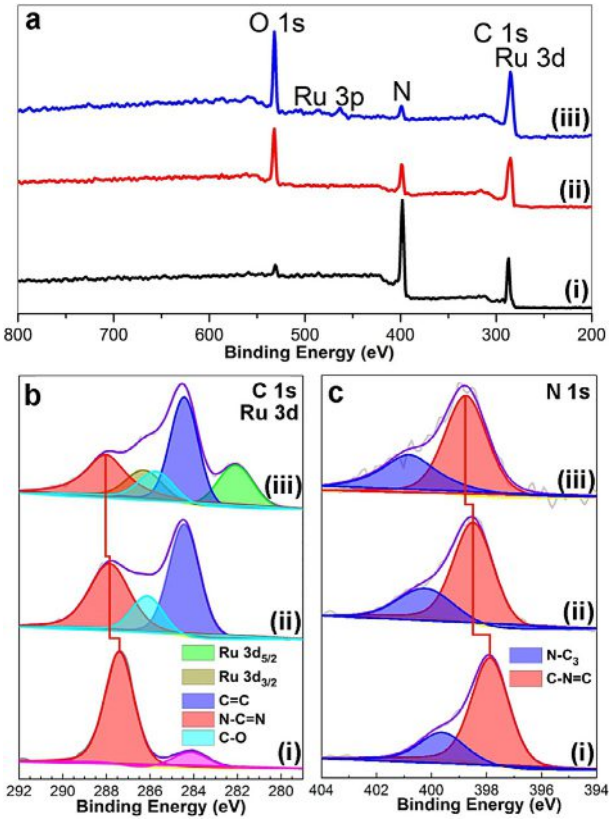

Figure 2. a) XPS survey spectra of (i) C3N4, (ii) C_3N_4/rGO, and (iii) Ru–C_3N_4/rGO. b) High-resolution XPS spectra of C 1s and Ru 3d electrons. c) High-resolution XPS spectra of N 1s electrons.

Significantly, the resulting Ru–C_3N_4/rGO nanocomposites exhibited high HER activity, which was markedly better than those of C_3N_4, C_3N_4/rGO, and Ru–C_3N_4 and comparable to that of Pt/C. Figure 3 a depicts the polarization curves in N_2-saturated 0.5 M H_2SO_4 of the various samples loaded onto a glassy carbon electrode, from which η_{10} can be estimated to be −416, −206, and −80 mV for C_3N_4, C_3N_4/rGO, and Ru–C_3N_4/rGO, respectively. Note that η_{10} for Ru–C_3N_4 was −140 mV.[24] Taken together, these results indicate that the embedding of ruthenium metal ions into the C_3N_4 matrix significantly increased the HER activity, and the performance may be further enhanced by the incorporation of rGO nanosheets. Significantly, the η_{10} for Ru–C_3N_4/rGO was also comparable to that of Pt/C (−41 mV). Consistent results can be obtained from analysis of the Tafel plots, which included the linear segments of the polarization curves (Figure 3 b). From the *y* axis intercept by linear regression, the exchange current density (J_0, Figure S2)

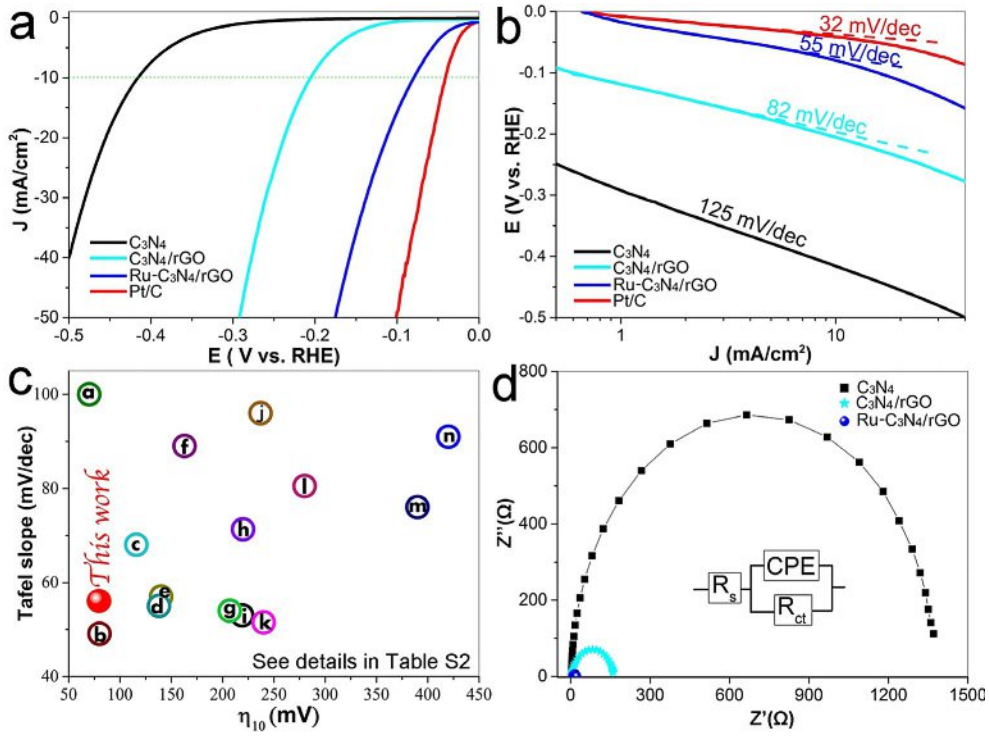

Figure 3. a) Polarization curves of HER on various electrocatalysts in 0.5 M H_2SO_4. b) Corresponding Tafel plots derived from panel (a). c) Comparison of the HER performance of the electrocatalysts in this work to other reported carbon-based catalysts (see Table S2 for details). d) Nyquist plots at an overpotential of −100 mV. Inset is the equivalent circuit of the electrocatalyst-coated electrode, where R_s is uncompensated resistance, R_{ct} is charge transfer resistance, and CPE is constant-phase element (equivalent to electrode double-layer capacitance, C_{dl}).

can be quantified to be 0.0045 mA cm^{-2} for C_3N_4, 0.036 mA cm^{-2} for C_3N_4/rGO, 0.072 mA cm^{-2} for Ru–C_3N_4,[24] and 0.462 mA cm^{-2} for Ru–C_3N_4/rGO. The Ru–C_3N_4/rGO performance is thus about 80% that of Pt/C (J_0 = 0.576 mA cm^{-2}), but roughly 6 times that of Ru–C_3N_4, 13 times that of C_3N_4/rGO, and 103 times that of C_3N_4. In fact, the Ru–C_3N_4/rGO showed a cathodic current density of 35.83 mA cm^{-2} which was 14.6 times that of C_3N_4/rGO (2.45 mA cm^{-2}) and 227 times of C_3N_4 (0.158 mA cm^{-2}) at an overpotential of −150 mV (Figure S3).

Additionally, the Ru–C_3N_4/rGO nanocomposite exhibited excellent durability. There was almost no change in the voltammetric profiles after 5000 cycles of potential scanning and chronoamperometric measurements for up to 9 h (Figure S4). Furthermore, the corresponding Tafel slope can be estimated to be 125 mV dec^{-1} for C_3N_4, 82 mV dec^{-1} for C_3N_4/rGO, 57 mV dec^{-1} for Ru–C_3N_4,[24] and 55 mV dec^{-1} for Ru–C_3N_4/rGO—the latter is, again, very comparable to that (32 mV dec^{-1}) of Pt/C. This suggests that hydrogen evolution catalyzed by Ru–C_3N_4/rGO likely followed a mechanism similar to that by Pt/C with the Volmer–Heyrovsky reaction being the rate-determining step.[42] The HER performance of Ru–C_3N_4/rGO is also drastically better than many other recently reported carbon-based catalysts listed in Figure 3c and Tables S2 and S3 (see the References therein).

Electrochemical impedance measurements were then carried out to evaluate the corresponding charge-transfer resistance (R_{ct}). Figure S5 shows the Nyquist plots of Ru–C_3N_4/rGO at various overpotentials, from which R_{ct} was quantified by fitting the data to the Randle's equivalent circuit (inset to Figure 3d) and found to decrease significantly with increasing overpotentials; 46.4 Ω at −50 mV, 19.7 Ω at −100 mV, 9.1 Ω at −150 mV, and 5.0 Ω at −200 mV. Figure 3d compares the Nyquist plots of the various samples at the same overpotential of −100 mV, where R_{ct} was estimated to be 1,366 Ω for C_3N_4, 157 Ω for C_3N_4/rGO, 88 Ω for Ru–C_3N_4,[24] and 20 Ω for Ru–C_3N_4/rGO. Therefore, the poor HER performance of C_3N_4 may be ascribed to its semiconducting nature and sluggish electron-transfer kinetics. However, the incorporation with rGO greatly facilitates the electron-transfer reaction with R_{ct} markedly reduced by over an order of magnitude. Further enhancement can be observed when ruthenium metal ions were embedded into the nanocomposites where R_{ct} was approximately 70 times smaller.

In the previous study with Ru–C_3N_4,[24] we observed that the incorporation of ruthenium metal ions into the C_3N_4 scaffold by Ru–N coordination bonds led to electron redistribution within the composites, which facilitated the adsorption of hydrogen and proton reduction to hydrogen. This formation of an increasing number of HER active sites can be evidenced in the corresponding effective electrochemical surface area, as reflected by the electrode double-layer capacitance (C_{dl}). Figure 4a shows the voltammograms of Ru–C_3N_4/rGO (data for C_3N_4 and C_3N_4/rGO are included in Figure S6, and those for Ru–C_3N_4 in our previous study[24]) at scan rates of 10–60 mV s^{-1} within a potential range of +0.1 to +0.2 V where no faradaic reaction occurred. As shown in Figure 4b, C_{dl} was estimated to

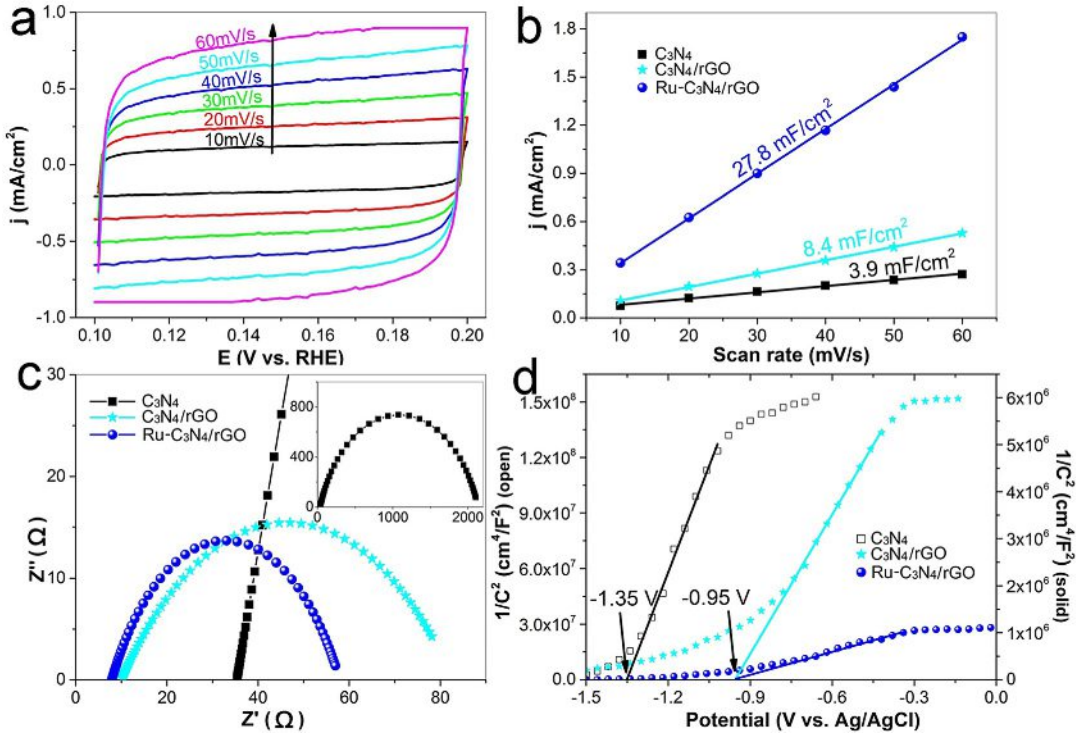

Figure 4. a) Cyclic voltammograms within the range of +0.1 V to +0.2 V where no faradaic reaction occurred at different scan rates. b) Variation of the double-layer charging currents at +0.15 V versus scan rate. c) Nyquist plots of electrocatalysts without carbon black collected in 0.5 M H_2SO_4 at the overpotential of −100 mV. Inset is the full plot of C_3N_4. d) Mott–Schottky plots of the various electrocatalysts collected in 0.1 M Na_2SO_4 at a frequency of 1000 Hz, where the potential is referred to an Ag/AgCl reference electrode. Note that C_3N_4 (open symbols) uses the left *y* axis, whereas C_3N_4/rGO and Ru–C_3N_4/rGO (solid symbols) use the right *y* axis.

be 27.8 mF cm^{-2} for Ru–C_3N_4/rGO, over 7 times that of C_3N_4 (3.9 mF cm^{-2}), 3 times that of C_3N_4/rGO (8.4 mF cm^{-2}), and 1.5 times that of Ru–C_3N_4 (18.4 mF cm^{-2}).[24] This dramatic enhancement of the effective electrochemical surface area might be ascribed to the enhanced electrical conductivity of the composite with the incorporation of rGO and Ru centers into C_3N_4. Indeed, from the Nyquist plots (Figure 4c), the uncompensated resistance R_s was estimated to be 35.4 Ω for C_3N_4, and markedly reduced to 10.0 Ω when rGO was incorporated to form C_3N_4/rGO, and further to 7.9 Ω in Ru–C_3N_4/rGO where ruthenium metal ions were embedded.

To unravel further insights into the HER performance, a Mott–Schottky analysis was performed. From Figure 4d, it can be clearly seen that all samples exhibited a positive slope, indicating n-type semiconducting nature of the C_3N_4-based materials.[39] Additionally, the flat-band potential (E_{fb}) of C_3N_4 was estimated to be −1.35 V (vs. Ag/AgCl), but shifted anodically to around −0.95 V for the other two. Thermodynamically, E_{fb} of an n-type semiconductor determines the conduction band position, and the positive shift of the conduction band suggests narrowing of the energy barrier of hydrogen evolution (H^+/H_2; −0.59 V vs. Ag/AgCl in 0.1 M Na_2SO_4), leading to enhanced electrocatalytic performance of the material.[43] Furthermore, the charge-carrier densities (N_d) of the catalysts can be calculated by Equation (1):

$$N_d = \frac{2}{e\,\varepsilon\,\varepsilon_0\,m} \quad (1)$$

where e is the elementary charge of an electron, ε is the dielectric constant (ca. 10 in the present study),[44] ε_0 is permittivity in a vacuum (8.85×10^{-12} F m^{-1}), and m is the slope of the Mott–Schottky plot. From Figure 4d, the charge-carrier densities were estimated to be 3.67×10^{15} cm^{-3} for C_3N_4, 1.42×10^{17} cm^{-3} for C_3N_4/rGO, and 9.05×10^{17} cm^{-3} for Ru–C_3N_4/rGO. That is, the charge-carrier density of Ru–C_3N_4/rGO is about 250 times of that C_3N_4 and 6 times of that C_3N_4/rGO. This observation is consistent with results from impedance and voltammetric measurements.

Conclusion

In summary, a new functional nanocomposite was prepared by embedding ruthenium metal ions into C_3N_4/rGO composites where the ruthenium centers were bonded to the pyridinic nitrogen of the carbon nitride scaffold. The resulting Ru–C_3N_4/rGO nanocomposites exhibited markedly enhanced electrocatalytic activity towards HER, with a low η_{10} of only −80 mV, a Tafel slope of 55 mV dec^{-1}, and an exchange current density of 0.462 mA cm^{-2}. This performance is markedly better than those of C_3N_4, C_3N_4/rGO, and Ru–C_3N_4 and is even comparable to that of commercial Pt/C. The impressive performance was accounted for by electron redistribution upon the incorporation of ruthenium ions into the C_3N_4/rGO composites, which led to efficient narrowing of the material band gap, enhanced electric conductivity and charge-carrier density, increased number of active sites, and reduced charge-transfer resistance. Such inter-

actions between the structural components (C_3N_4, rGO, and Ru ions) facilitate an effective strategy in the rational design and engineering of functional composites in the development of high-performance HER electrocatalysts.

Experimental Section

Chemicals

Melamine (99%, Acros), ruthenium chloride ($RuCl_3$, 35–40% Ru, Acros), sulfuric acid (H_2SO_4, 98%, Fisher Chemicals), sodium chloride (NaCl, 99%, Acros), sodium nitrate ($NaNO_3$, 99%, Acros), potassium permanganate ($KMnO_4$, 99%, Fisher Chemicals), and ascorbic acid (99%, Fisher Chemicals) were used as received. All solvents were obtained from typical commercial sources and used without further treatment. Water was supplied by a Barnstead Nanopure water system (18.3 MΩ cm).

Synthesis of graphitic carbon nitride

C_3N_4 was synthesized by direct pyrolysis of melamine in air.[27,28] Briefly, melamine (10 g) was placed in a crucible with a cover and then heated at 600 °C for 3 h. After being cooled down to room temperature, the yellow product was collected and ground to fine powder. 50 mg of the obtained C_3N_4 powder was then mixed with Nanopure H_2O (50 mL) under sonication overnight to produce well-dispersed thin-layer C_3N_4.

Synthesis of graphene oxide

GO was synthesized by a modified Hummers method.[25,26] In a typical experiment, graphite flakes (1 g) were ground with NaCl (20 g) for 15 min, and NaCl was washed away by rinsing with water in a vacuum filtration apparatus. The remaining graphite was dried in an oven at 70 °C, and then transferred to a 250 mL round-bottom flask. Concentrated H_2SO_4 (23 mL) was added into the flask and the mixture was stirred at room temperature for 24 h before being heated in an oil bath at 40 °C. $NaNO_3$ (100 mg) was added to the suspension and allowed to dissolve in 5 min. This step was followed by the slow addition of $KMnO_4$ (3 g), with the solution temperature kept below 45 °C, under magnetic stirring for 30 min. The flask was removed from the oil bath and Nanopure water (140 mL) and 30% H_2O_2 (10 mL) were added to the reaction. The mixture was under magnetic stirring at room temperature for 5 min. It was then repeatedly centrifuged and washed with 5% HCl solution twice, followed by rinsing with copious amounts of water. The final precipitate was dispersed in water (100 mL) and sonicated for 30 min. Insoluble solids were removed by centrifugation at 3000 rpm for 5 min, and the brown supernatant was collected and dried in an oven at 70 °C.

Synthesis of C_3N_4/rGO composites

C_3N_4/rGO composites were synthesized by following a reported protocol.[20,21,29] In brief, GO (50 mg) was added into a 1 mg mL^{-1} thin-layer C_3N_4 solution (50 mL; see above for preparation). The mixture was sonicated for 1 h before being heated at reflux with ascorbic acid (176 mg) for 2 h. The products were collected by centrifugation.

Synthesis of Ru–C_3N_4/rGO complexes

To synthesize Ru–C_3N_4/rGO hybrids, the C_3N_4/rGO composites obtained above were dispersed in Nanopure H_2O, (50 mL) into which was then added $RuCl_3$ (28 mg). The mixture was heated at reflux for 2 h . The product was collected by centrifugation at 4500 rpm for 10 min and washed with H_2O and ethanol (2×20 mL). At this feed ratio, the supernatant showed a light brown color, indicating that there was a small excess of ruthenium ions in the solution and C_3N_4 was saturated with ruthenium complexation.[24]

Characterization

The morphology of the samples was characterized by transmission electron microscopy (TEM; Philips CM300 at 300 kV) and atomic force microscopy (AFM; Molecular Imaging PicoLE SPM). The samples were prepared by dropcasting a dilute dispersion of the nanocomposites in ethanol onto a TEM grid or clean mica surface, and dried in a vacuum oven. X-ray photoelectron spectroscopic (XPS) measurements were carried out with a PHI 5400/XPS instrument equipped with an $Al_{K\alpha}$ source operated at 350 W and 10^{-9} torr.

Electrochemistry

Electrochemical tests were performed using a CHI710 workstation and electrochemical impedance and Mott–Schottky measurements were carried out with a Gamry Reference 600 instrument. A Ag/AgCl electrode (1 M KCl) and Pt wire were used as the reference electrode and counter electrode, respectively and a glassy carbon electrode (5 mm in diameter, 0.196 cm^2) was used as the working electrode. The Ag/AgCl electrode was calibrated against a reversible hydrogen electrode (RHE), and all potentials were referred to this RHE except for the Mott–Schottky analysis, where the potential was referenced to Ag/AgCl. To prepare catalyst inks, 2 mg of the catalysts (obtained as described above) and 3 mg of carbon black were dispersed in 1 mL of a 1:4 v/v water/ethanol mixed solvents along with 10 μL of a Nafion solution, and the mixture was sonicated for 30 min to achieve good dispersion of the materials. Then 15 μL of the above inks was dropcast onto the surface of the glassy carbon electrode and dried at room temperature, corresponding to a mass loading of 0.153 mg cm^{-2} for the catalysts. All measurements were carried out in 0.5 M H_2SO_4 except for Mott–Schottky analysis, which was performed in 0.1 M Na_2SO_4.

Acknowledgements

This work was supported, in part, by the National Science Foundation (DMR-1409396 and CHE-1710408) and by the Merced nAnomaterials Center for Energy and Sensing (MACES), a NASA funded MIRO center, under award NNX15AQ01. TEM and XPS studies were carried out at the National Center for Electron Microscopy and Molecular Foundry of the Lawrence Berkeley National Laboratory, which is supported by the US Department of Energy, as part of a user project.

Conflict of interest

The authors declare no conflict of interest.

Keywords: carbon nitride · electrocatalysis · Mott–Schottky analysis · graphene · ruthenium

[1] J. Greeley, T. F. Jaramillo, J. Bonde, I. B. Chorkendorff, J. K. Norskov, *Nat. Mater.* **2006**, *5*, 909 – 913.
[2] M. Cabán-Acevedo, M. L. Stone, J. R. Schmidt, J. G. Thomas, Q. Ding, H. C. Chang, M. L. Tsai, J. H. He, S. Jin, *Nat. Mater.* **2015**, *14*, 1245 – 1251.
[3] P. W. Du, R. Eisenberg, *Energy Environ. Sci.* **2012**, *5*, 6012 – 6021.
[4] C. C. L. McCrory, S. Jung, I. M. Ferrer, S. M. Chatman, J. C. Peters, T. F. Jaramillo, *J. Am. Chem. Soc.* **2015**, *137*, 4347 – 4357.
[5] B. E. Conway, B. V. Tilak, *Electrochim. Acta* **2002**, *47*, 3571 – 3594.
[6] E. J. Popczun, J. R. McKone, C. G. Read, A. J. Biacchi, A. M. Wiltrout, N. S. Lewis, R. E. Schaak, *J. Am. Chem. Soc.* **2013**, *135*, 9267 – 9270.
[7] C. G. Morales-Guio, L. A. Stern, X. L. Hu, *Chem. Soc. Rev.* **2014**, *43*, 6555 – 6569.
[8] Y. Yan, B. Y. Xia, Z. C. Xu, X. Wang, *ACS Catal.* **2014**, *4*, 1693 – 1705.
[9] D. Voiry, J. Yang, M. Chhowalla, *Adv. Mater.* **2016**, *28*, 6197 – 6206.
[10] B. Kumar, M. Asadi, D. Pisasale, S. Sinha-Ray, B. A. Rosen, R. Haasch, J. Abiade, A. L. Yarin, A. Salehi-Khojin, *Nat. Commun.* **2013**, *4*, 2819.
[11] X. J. Zhou, J. L. Qiao, L. Yang, J. J. Zhang, *Adv. Energy Mater.* **2014**, *4*, 1301523.
[12] J. J. Duan, S. Chen, M. Jaroniec, S. Z. Qiao, *ACS Catal.* **2015**, *5*, 5207 – 5234.
[13] J. S. Zhang, Y. Chen, X. C. Wang, *Energy Environ. Sci.* **2015**, *8*, 3092 – 3108.
[14] C. G. Hu, L. M. Dai, *Angew. Chem. Int. Ed.* **2016**, *55*, 11736 – 11758; *Angew. Chem.* **2016**, *128*, 11910 – 11933.
[15] J. T. Zhang, H. L. Li, P. Z. Guo, H. Y. Ma, X. S. Zhao, *J. Mater. Chem. A* **2016**, *4*, 8497 – 8511.
[16] S. S. Shinde, A. Sami, J. H. Lee, *ChemCatChem* **2015**, *7*, 3873 – 3880.
[17] S. S. Shinde, A. Sami, D. H. Kim, J. H. Lee, *Chem. Commun.* **2015**, *51*, 15716 – 15719.
[18] S. S. Shinde, A. Sami, J. H. Lee, *J. Mater. Chem. A* **2015**, *3*, 12810 – 12819.
[19] M. Chhetri, S. Maitra, H. Chakraborty, U. V. Waghmare, C. N. R. Rao, *Energy Environ. Sci.* **2016**, *9*, 95 – 101.
[20] Y. Zheng, Y. Jiao, Y. Zhu, L. H. Li, Y. Han, Y. Chen, A. Du, M. Jaroniec, S. Z. Qiao, *Nat. Commun.* **2014**, *5*, 3783.
[21] Y. Zhao, F. Zhao, X. P. Wang, C. Y. Xu, Z. P. Zhang, G. Q. Shi, L. T. Qu, *Angew. Chem. Int. Ed.* **2014**, *53*, 13934 – 13939; *Angew. Chem.* **2014**, *126*, 14154 – 14159.
[22] J. J. Duan, S. Chen, M. Jaroniec, S. Z. Qiao, *ACS Nano* **2015**, *9*, 931 – 940.
[23] Q. Han, Z. Chen, J. Gao, Y. Zhao, Z. Zhang, L. Dai, L. Qu, *Adv. Funct. Mater.* **2017**, *27*, 1606352.
[24] Y. Peng, B. Lu, L. Chen, N. Wang, J. E. Lu, Y. Ping, S. Chen, *J. Mater. Chem. A* **2017**, *5*, 18261 – 18269.
[25] S. Gilje, S. Han, M. Wang, K. L. Wang, R. B. Kaner, *Nano Lett.* **2007**, *7*, 3394 – 3398.
[26] L. J. Cote, F. Kim, J. X. Huang, *J. Am. Chem. Soc.* **2009**, *131*, 1043 – 1049.
[27] J. Tian, Q. Liu, C. Ge, Z. Xing, A. M. Asiri, A. O. Al-Youbi, X. Sun, *Nanoscale* **2013**, *5*, 8921 – 8924.
[28] X. Zhang, X. Xie, H. Wang, J. Zhang, B. Pan, Y. Xie, *J. Am. Chem. Soc.* **2013**, *135*, 18 – 21.
[29] A. J. Du, S. Sanvito, Z. Li, D. W. Wang, Y. Jiao, T. Liao, Q. Sun, Y. H. Ng, Z. H. Zhu, R. Amal, S. C. Smith, *J. Am. Chem. Soc.* **2012**, *134*, 4393 – 4397.
[30] A. K. Geim, I. V. Grigorieva, *Nature* **2013**, *499*, 419 – 425.
[31] W. J. Ong, L. L. Tan, S. P. Chai, S. T. Yong, A. R. Mohamed, *Nano Energy* **2015**, *13*, 757 – 770.
[32] W. C. Wan, S. Yu, F. Dong, Q. Zhang, Y. Zhou, *J. Mater. Chem. A* **2016**, *4*, 7823 – 7829.
[33] X. W. Kang, S. W. Chen, *Nanoscale* **2012**, *4*, 4183 – 4189.
[34] J. Liu, Y. Liu, N. Y. Liu, Y. Z. Han, X. Zhang, H. Huang, Y. Lifshitz, S. T. Lee, J. Zhong, Z. H. Kang, *Science* **2015**, *347*, 970 – 974.
[35] S. W. Cao, J. Jiang, B. C. Zhu, J. G. Yu, *Phys. Chem. Chem. Phys.* **2016**, *18*, 19457 – 19463.
[36] I. K. Moon, J. Lee, R. S. Ruoff, H. Lee, *Nat. Commun.* **2010**, *1*, 73.
[37] C. Creutz, N. Sutin, *Proc. Natl. Acad. Sci. USA* **1975**, *72*, 2858 – 2862.
[38] L. M. Chen, P. G. Hu, C. P. Deming, N. Wang, J. E. Lu, S. W. Chen, *J. Phys. Chem. C* **2016**, *120*, 13303 – 13309.
[39] S. B. Yang, Y. J. Gong, J. S. Zhang, L. Zhan, L. L. Ma, Z. Y. Fang, R. Vajtai, X. C. Wang, P. M. Ajayan, *Adv. Mater.* **2013**, *25*, 2452 – 2456.
[40] V. Q. Nguyen, X. N. Sun, F. Lafolet, J. F. Audibert, F. Miomandre, G. Lemercier, F. Loiseau, J. C. Lacroix, *J. Am. Chem. Soc.* **2016**, *138*, 9381 – 9384.
[41] X. Tan, H. A. Tahini, S. C. Smith, *ACS Catal.* **2016**, *6*, 7071 – 7077.
[42] L. J. Yang, W. J. Zhou, J. Lu, D. M. Hou, Y. T. Ke, G. Q. Li, Z. H. Tang, X. W. Kang, S. W. Chen, *Nano Energy* **2016**, *22*, 490 – 498.
[43] J. S. Zhang, X. F. Chen, K. Takanabe, K. Maeda, K. Domen, J. D. Epping, X. Z. Fu, M. Antonietti, X. C. Wang, *Angew. Chem. Int. Ed.* **2010**, *49*, 441 – 444; *Angew. Chem.* **2010**, *122*, 451 – 454.
[44] F. H. Abd El-kader, M. A. Moharram, M. G. Khafagia, F. Mamdouh, *Spectrochim. Acta* **2012**, *97*, 1115 – 1119.

Manuscript received: October 4, 2017
Revised manuscript received: October 31, 2017
Accepted manuscript online: November 9, 2017
Version of record online: December 5, 2017